

Self-homodyne wavelength locking of a silicon microring resonator

QINGMING ZHU,  CIYUAN QIU, *  YU HE,  YONG ZHANG, AND YIKAI SU 

State Key Lab of Advanced Optical Communication Systems and Networks, Department of Electronic Engineering, Shanghai Jiao Tong University, Shanghai 200240, China

* qiuciyuan@sjtu.edu.cn

Abstract: We propose and experimentally demonstrate a self-homodyne locking method for a silicon microring resonator (MRR). The device employs a self-homodyne detection structure and consists of a tunable MRR with two directional couplers along the ring for monitoring, two phase shifters to calibrate the phase difference between the two monitored optical signals, and a Y-branch to combine the two signals. A single photodetector is used to detect the output power of the Y-branch. If the MRR is on resonance, a destructive interference occurs in the Y-branch, therefore the monitored photocurrent is minimized. By using such a device structure and the homodyne detection scheme, the MRR with a Q factor of 1.9×10^4 can be accurately locked to the signal wavelength, and the locking process is insensitive to input power variation. The wavelength locking range is larger than one free spectral range (FSR) of 6 nm, and the locking errors are ≤ 0.015 nm.

© 2019 Optical Society of America under the terms of the [OSA Open Access Publishing Agreement](#)

1. Introduction

Photonic devices and integrated circuits have been advancing rapidly during the past decades, and resonators play an important role in the progresses [1,2]. Owing to their spectral selectivity, compact footprints, and low power consumption, resonators can be used for lasers, filters, switches, modulators, wavelength multiplexers/demultiplexers, and so on [2–5]. Among them, the lasers usually suffer from frequency fluctuations induced by thermal variations and the elasto-optic effect [5]. To realize the frequency stabilization of a laser, many approaches have been proposed and demonstrated, including the widely used Pound-Drever-Hall method [5–7] and the efficient self-injection locking method [8,9]. The other resonant devices, e.g., silicon microring filters, also suffer from susceptibility to fabrication errors and chip temperature variations, resulting in wavelength misalignments between the resonance wavelengths and the signal wavelengths. In practical applications, the problem of the wavelength misalignments needs to be solved by automated wavelength locking methods [2–4].

For the wavelength locking of a silicon resonator, the basic principle is to monitor a device/system parameter which varies as a function of the wavelength misalignment and then to tune the resonator according to the monitored signal. Such a parameter can be power transmission [10–21], round-trip phase shift (RTPS) [22,23], bit-error rate [24], temperature [25], etc. In general, a wavelength locking method is expected to exhibit a wide locking range, a fast locking speed, simple control photonics and electronics, and insensitivity to thermal crosstalk and input power variation. The wavelength locking range and the locking speed can be improved through optimizations of the device and the control subsystem, while the other goals typically need to be achieved by new device structures or control algorithms. However, the input-power variation issue has been rarely addressed in the wavelength locking methods [10–25].

In this paper, we propose and experimentally demonstrate a self-homodyne locking (SHL) method for a silicon microring resonator (MRR). The SHL method employs a new device structure to realize RTPS monitoring using a single photodetector, and this method is insensitive

to the input power variation. The device is composed of an MRR integrated with a micro-heater for the thermo-optic (TO) tuning, two directional couplers along the ring, two phase shifters, and a Y-branch. Two waveguided optical beams are coupled out of the ring and then passed through the phase shifters. The two optical beams can possess nearly the same intensities with a proper device design, but their phase difference is highly susceptible to fabrication errors and needs to be calibrated by the phase shifters. After the phase calibration, the two optical beams are combined by the Y-branch and then sent to a photodetector. If the MRR is locked to the signal wavelength, a minimal photocurrent can be obtained due to the destructive interference of the two optical beams. To realize the wavelength locking, a control subsystem is then used to automatically adjust the heating powers applied to the MRR and the phase shifter, according to the monitored photocurrent. Here, we perform two proof-of-concept experiments to verify that: 1) the MRR can be accurately locked to any signal wavelength within a free spectral range (FSR); 2) the SHL method is insensitive to a large input optical power variation. The demonstrated wavelength locking range is >6 nm, and the locking errors are ≤ 0.015 nm. With the power-variation insensitivity, the wide locking range, and the simple control photonics, the proposed SHL method appears desirable for MRR-based devices.

2. Operation principle

Figure 1 depicts the schematic diagram of this method. The device includes an MRR, two phase shifters, and a Y-branch. The MRR is integrated with a micro-heater and two directional couplers. The directional couplers are placed symmetrically with respect to the center of the ring. A waveguided optical beam is fed into the device, coupled into the ring with the coupling coefficient denoted as k_1 , and is then coupled out by the directional couplers with the same coupling coefficient denoted as k_2 . The electric fields of the input light and the output light at the through port are denoted by E_{in} and E_{thru} , respectively. Using a transfer matrix method [26], the electric fields of the two monitored optical beams at M1 and M2 are expressed as

$$\begin{bmatrix} E_{M2} \\ E_{M1} \end{bmatrix} = \begin{bmatrix} ik_2/t_2 & 0 \\ 0 & ik_2 \end{bmatrix} \begin{bmatrix} a_{ring}^{-1/4} & 0 \\ 0 & a_{ring}^{1/4} \end{bmatrix} \frac{1}{ik_1} \begin{bmatrix} -t_1 & 1 \\ -1 & t_1 \end{bmatrix} \begin{bmatrix} E_{in} \\ E_{thru} \end{bmatrix}, \quad (1)$$

$$E_{M2} = t_2 a_{ring}^{1/2} E_{M1}, \quad (2)$$

$$\begin{aligned} a_{ring} &= \exp(-\alpha L_{ring} - j\beta L_{ring}) \\ &= \exp(-\alpha L_{ring} - j2m\pi - j2\pi n_g L_{ring} \Delta\lambda / \lambda^2), \end{aligned} \quad (3)$$

where t_i ($t_i^2 + k_i^2 = 1$, $i = 1, 2$) are the transmission coefficients of the directional couplers, a_{ring} represents the transmission factor along the ring, α and β are the loss factor and the propagation constant of the waveguides, respectively, L_{ring} is the circumference of the ring, m is an integer, n_g is the group index, λ is the signal wavelength, λ_{res} is the m -th resonance wavelength of the MRR, and $\Delta\lambda = \lambda_{res} - \lambda$ is the wavelength misalignment. Combining Eqs. (1–3) leads to

$$E_{M1} = -k_1 k_2 \frac{a_{ring}^{1/4}}{1 - t_1 t_2^2 a_{ring}} E_{in}, \quad (4)$$

$$\begin{aligned} E_{M2} &= t_2 \exp(-\alpha L_{ring}/2) \exp(-j\beta L_{ring}/2) E_{M1} \\ &\approx E_{M1} \exp(-j m\pi - j\pi n_g L_{ring} \Delta\lambda / \lambda^2). \end{aligned} \quad (5)$$

By properly designing the gap parameters of the MRR, $t_2 \exp(-\alpha L_{ring}/2)$ is approximately equal to 1, i.e., $|E_{M1}| \approx |E_{M2}|$ is satisfied. Therefore, the intensities of the two monitored optical

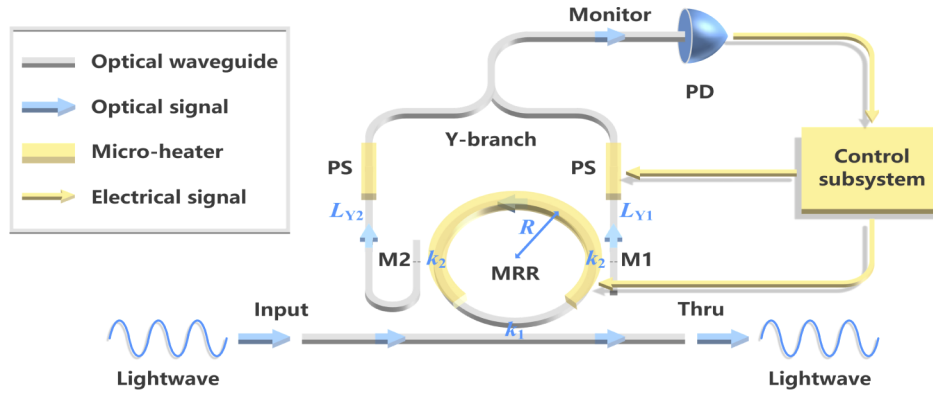


Fig. 1. Schematic diagram of the SHL method. MRR: microring resonator. PS: phase shifter. PD: photodetector.

beams are nearly the same. Meanwhile, the phase difference between the two light beams is related to m and $\Delta\lambda$, according to Eq. (5).

The two light beams with similar intensities and different phases are combined in the Y-branch. The transmission factors along the two arms of the Y-branch are denoted by a_{Y1} and a_{Y2} , respectively. Note that, as shown in Fig. 1, the phases of a_{Y1} and a_{Y2} can be tuned by the corresponding phase shifters, respectively. Assuming equal lengths of the two arms of the Y-branch, $a_{Y1} = a_{Y2}$ is satisfied. The electric field of the optical beam at the output port of the Y-branch, denoted as the monitoring port, is given by:

$$\begin{aligned} E_{monitor} &= \frac{1}{\sqrt{2}} (a_{Y1} E_{M1} + a_{Y2} E_{M2}) \\ &\approx \frac{1}{\sqrt{2}} a_{Y1} E_{M1} (1 + \exp(-j m \pi - j \pi n_g L_{ring} \Delta\lambda / \lambda^2)). \end{aligned} \quad (6)$$

Hence, the two light beams can interfere either destructively or constructively in the Y-branch at $\Delta\lambda = 0$, depending on m . In this locking method, a destructive interference is required, so m is chosen to be an odd number. Then, $|E_{monitor}|^2$, which is proportional to the output power of the Y-branch, is expressed as:

$$\begin{aligned} |E_{monitor}|^2 &= T_{monitor}(\Delta\lambda) |E_{in}|^2 \\ &\approx \frac{1}{2} k_1^2 k_2^2 \left| \frac{a_{Y1} a_{ring}^{1/4}}{1 - t_1 t_2^2 a_{ring}} \right|^2 |1 - \exp(-j \pi n_g L_{ring} \Delta\lambda / \lambda^2)|^2 |E_{in}|^2. \end{aligned} \quad (7)$$

$T_{monitor}(\Delta\lambda)$ is defined as the power transmission function from the input port to the monitoring port. According to Eq. (7), $T_{monitor}(\Delta\lambda)$ is close to zero at $\Delta\lambda = 0$. Therefore, $|E_{monitor}|^2$ is always kept at the minimal level if the MRR is locked to the signal wavelength, and large (e.g., 10-dB) variation of $|E_{in}|^2$ would not affect the wavelength locking process. Note that, this method can also be employed in the case where m is an even number. In that case, a minimum output power can still be obtained at $\Delta\lambda = 0$ if $a_{Y1} = -a_{Y2}$ is obtained by tuning the phase shifters.

The output power of the Y-branch is then detected by a single photodetector. Since the photocurrent is proportional to the optical power, the current is minimized as long as the MRR is locked to the signal wavelength with $\Delta\lambda = 0$. Thus, the monitored photocurrent can be used as the feedback control signal for the control subsystem, as shown in Fig. 1.

To further illustrate the principle, the simulated transmissions of such a device versus $\Delta\lambda$ at both the through and monitoring ports are provided in Fig. 2. Here, the ring radius is $15\ \mu\text{m}$. The lengths of the two arms are assumed to be $173.3\ \mu\text{m}$. m is an odd number. Other simulation parameters are $k_1 = 0.221$, $k_2 = 0.077$, $\alpha = 1.75\ \text{cm}^{-1}$, $n_g = 4.2486$. For the transmission spectrum at the monitoring port, a notch with the transmission of $< -50\ \text{dB}$ is observed at $\Delta\lambda = 0$, indicating an effective destructive interference of the two monitored optical beams. Therefore, if the wavelength misalignment is eliminated, the optical power at the monitoring port is minimized. Meanwhile, a maximum monitoring power is observed if the wavelength misalignment is $\pm 6.0\ \text{nm}$, i.e., $\Delta\lambda = \pm\text{FSR} = \pm\lambda^2/n_g L_{\text{ring}}$ is satisfied. In that case, $\exp(-j\pi n_g L_{\text{ring}} \Delta\lambda/\lambda^2)$ is equal to -1 , so $T_{\text{monitor}}(\Delta\lambda)$ is maximized according to Eq. (7).

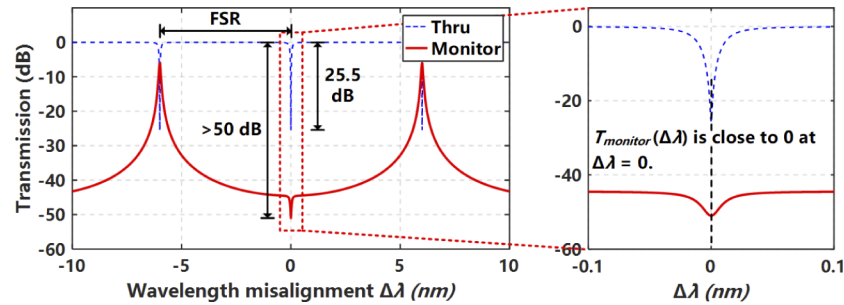


Fig. 2. Simulated transmission spectra at the through and monitoring ports. $\Delta\lambda$ is the wavelength misalignment. $T_{\text{monitor}}(\Delta\lambda)$ is the power transmission function from the input port to the monitoring port.

Based on the device structure discussed above, the MRR can be then locked by a control subsystem with the schematic diagram depicted in Fig. 3(a). In the subsystem, the monitored photocurrent is amplified by a trans-impedance amplifier (TIA), sampled by an analog-to-digital converter (ADC), and is then sent to the digital signal processor. The processor controls the heating power applied to the MRR through a digital-to-analog converter (DAC) and a driver. In the process, the basic idea is to tune the MRR to minimize the monitored photocurrent at the signal wavelength. Note that, the phase shifts in the two arms of the Y-branch can be affected by fabrication errors as well as the thermal crosstalk from the MRR under the TO tuning. To compensate these effects in the wavelength locking process, the processor also simultaneously controls the heating power applied to one of the two phase shifters through a DAC and a driver, as shown in Fig. 3(a). Then, in the wavelength locking process, $a_{\gamma 1} = a_{\gamma 2}$ is always satisfied.

The control algorithm of the control subsystem is similar to that in [19]. A global minimum searching sub-process is first executed, as shown in Fig. 3(b). In the process, the heating power applied to the MRR (P_{MRR}) increases from 0 to the maximal heating power P_{max} with a fixed step size of ΔP . Here, this thermo-optic tuning range is larger than one FSR. In each step, the photocurrent I_{PD} is recorded. Afterwards, P_{MRR} is set to the power that gives the recorded minimal I_{PD} (denoted as $I_{\text{PD_min}}$). Note that, if no thermoelectric cooler is used, the chip temperature may drift over several seconds. This temperature drift in turn induces an additional wavelength misalignment throughout the locking process. Thus, the I_{PD} measured in the end of the global minimum searching may be larger than $I_{\text{PD_min}}$.

To address the temperature drift issue for long-term stabilization, a local minimum searching sub-process is then followed. The photocurrent measured in the previous tuning step is denoted by I_{PD}' . In each step, P_{MRR} changes by ΔP , then I_{PD} is measured and compared with I_{PD}' . If the photocurrent becomes smaller, the sign of ΔP remains unchanged. Otherwise, the sign is inverted. The step size $|\Delta P|$ is the same as that in the global minimum searching sub-process. Such a step is periodically performed to track the local minimum.

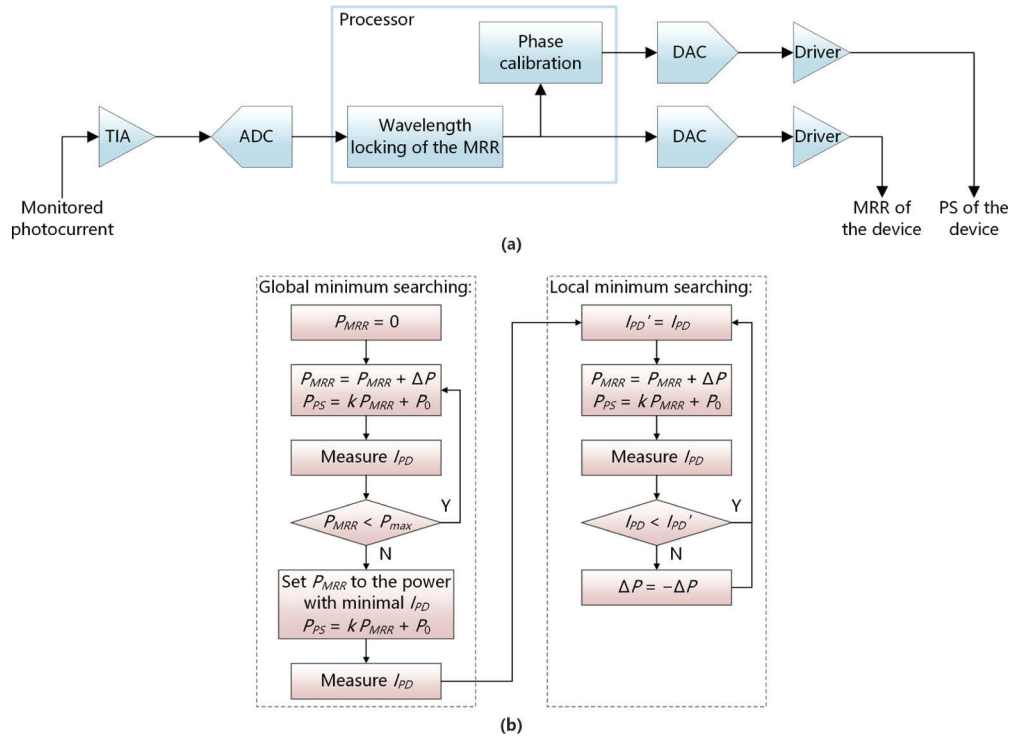


Fig. 3. (a) Schematic diagram of the control subsystem. (b) Flow chart of the control algorithm.

Furthermore, as shown in Fig. 3(b), the heating power (P_{PS}) on one of the two phase shifters is also updated in each tuning step of the two sub-processes to compensate the fabrication errors and the thermal crosstalk effects. Here, P_{PS} varies according to P_{MRR} as follows to obtain $a_{Y1} = a_{Y2}$:

$$P_{PS} = k P_{MRR} + P_0, \quad (8)$$

where k and P_0 are two constants related to the thermal crosstalk effects and fabrication errors, respectively. The two constants can be experimentally measured by a pre-calibration process, which will be demonstrated in Section 3.

3. Experimental verifications

3.1. Device design, fabrication, and control subsystem implementation

The device layout is shown in Fig. 4(a). The ring radius is $15 \mu\text{m}$. The gap between the ring and the bus waveguide is 150 nm , and the gaps between the ring and the two directional couplers are 270 nm . The two arms of the Y-branch possess nearly the same waveguide lengths of $173.3 \mu\text{m}$ (left arm) and $172.4 \mu\text{m}$ (right arm), respectively. Figure 4(b) is the micrograph of the fabricated device. The device was fabricated on a silicon-on-insulator (SOI) wafer with a 220-nm -thick top silicon layer. E-beam lithography (EBL, Vistec EBPG 5200+) was used to define the device pattern. The top silicon layer was etched by an inductively coupled plasma (ICP) etching process. A $1\text{-}\mu\text{m}$ -thick SiO_2 layer was then deposited on the whole device by plasma enhanced chemical vapor deposition (PECVD). 100-nm -thick Ti heaters and $1\text{-}\mu\text{m}$ -thick Al pads were fabricated using EBL and lift-off processes. The footprint of the device is $820 \mu\text{m} \times 700 \mu\text{m}$. The electrical resistances of the micro-heaters on the MRR and the phase shifters are $1.21 \text{ K}\Omega$ and $0.51 \text{ K}\Omega$,

respectively. The wavelength tuning efficiency of the MRR is 0.21 nm/mW. A heating power of ~ 14 mW is required to achieve a π -phase shift for the phase shifters.

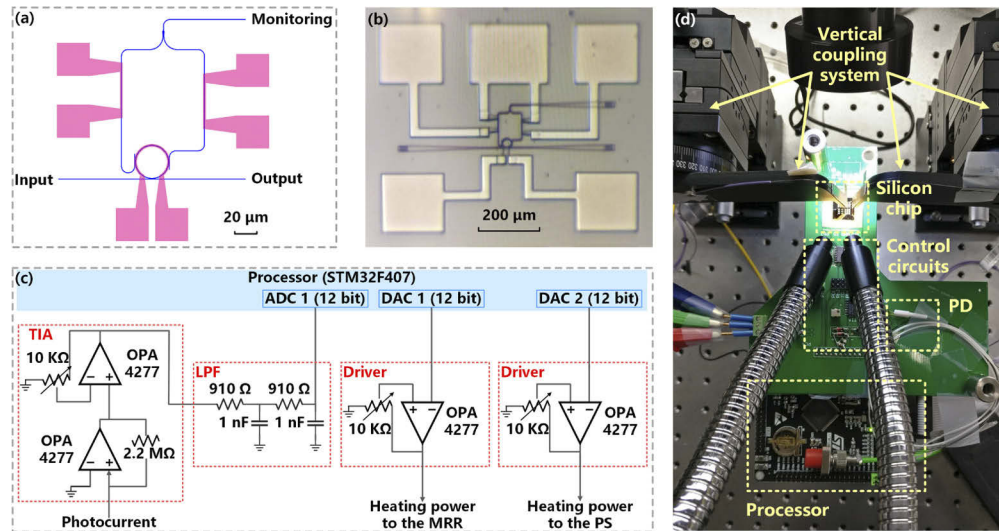


Fig. 4. (a) Device layout. (b) Micrograph of the device. (c) Detailed control circuitry of the subsystem. (d) Photograph of the control and coupling subsystems.

The fabricated device is then wire-bonded to the control circuits, with the detailed control circuitry depicted in Fig. 4(c). A commercial photodetector (PDCS986) with a bandwidth of 200 MHz and a responsivity of 0.84 A/W in C band is used to detect the monitored optical signal. The TIA is composed of two stages and has a total gain of 1.19×10^8 V/A. The output signal is passed through a 2nd-order low-pass filter (LPF), which can reduce the noise amplitude to 10 mV_{rms}. The filtered signal is sent to a commercial single-core processor (STM32F407) integrated with 12-bit ADCs and DACs. The control algorithm is implemented via C code. Here, P_{max} is set to be 34 mW to achieve a wavelength tuning range larger than one FSR, and ΔP is $P_{max}/1024 = 0.033$ mW. The thermal control period of each step is 73 μ s. The photograph of the control and coupling subsystems is shown in Fig. 4(d). Vertical coupling is used to couple the optical beams into and out of the device, with a coupling loss of ~ 7 dB/facet.

3.2. Self-homodyne locking over a full FSR

A proof-of-concept experiment was conducted to verify the feasibility of the proposed SHL method in a wide wavelength range. Figure 5 shows the experimental setup. A continuous wave (CW) light beam from a tunable C-band laser (Keysight 81960A) is adjusted to be TE-polarized by a polarization controller (PC) and is then injected into the device under test (DUT). A variable optical attenuator (VOA) is inserted before the DUT to decrease the optical power to 0 dBm, thus avoiding the thermal nonlinear effect [27,28]. The two output light beams at the through and monitoring ports are coupled out. Limited by the coupling system, we measured one output optical signal at a time. The optical signal is split into two parts using a 3-dB optical coupler. One part is fed into a Labview-controlled power meter (Keysight 81636B) to obtain the transmission spectra, and the other part is detected by the 200-MHz photodetector. The monitored photocurrent is sent to the control subsystem for feedback control. Note that, the relative intensity noise (RIN) of the laser is usually ~ -150 dBc/Hz over the frequency range from direct current (DC) to several GHz. Considering a bandwidth of ~ 10 GHz, the noise amplitude of the monitored signal induced

by the RIN is therefore five orders of magnitude lower than the monitored signal, so the RIN of the laser would not affect the wavelength locking process.

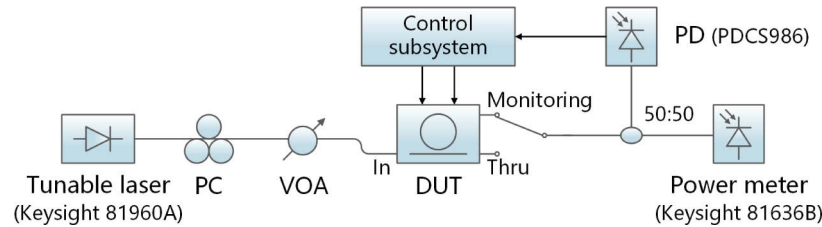


Fig. 5. Experimental setup for wide-range wavelength locking. PC: polarization controller. VOA: variable optical attenuator. DUT: device under test.

In the experiment, a phase pre-calibration process is performed before the automated wavelength locking. In the process, several heating powers P_{MRR} are applied to the MRR in order. For each P_{MRR} , we tune P_{PS} and then measure the transmission using the tunable laser. If a spectral notch is observed at the resonance wavelength, the values of P_{MRR} and P_{PS} are recorded to calculate the two constants k and P_0 through linear fitting, which are -0.121 and 11.16 mW, respectively. The transmission spectrum can also be measured with a single frequency laser [29]. In that case, the resonance wavelength of the MRR is tuned by adjusting P_{MRR} , thus avoiding the use of the tunable laser. Therefore, an alternative phase calibration method is to measure the transmission as a function of P_{PS} and P_{MRR} at a single signal wavelength. Both P_{MRR} and P_{PS} are properly set if a notch is observed in the two-dimensional transmission map.

The wavelength locking process can then be carried out. Here, the initial resonance wavelength of the MRR and the signal wavelength are 1543.808 nm and 1545 nm, respectively. The heating powers and the monitored signal during the locking process are recorded by the processor. As shown in Fig. 6(a), P_{MRR} increases step by step in the global minimum searching. A global minimum is located at 13.4 ms. Meanwhile, one can find that the voltage of the monitored

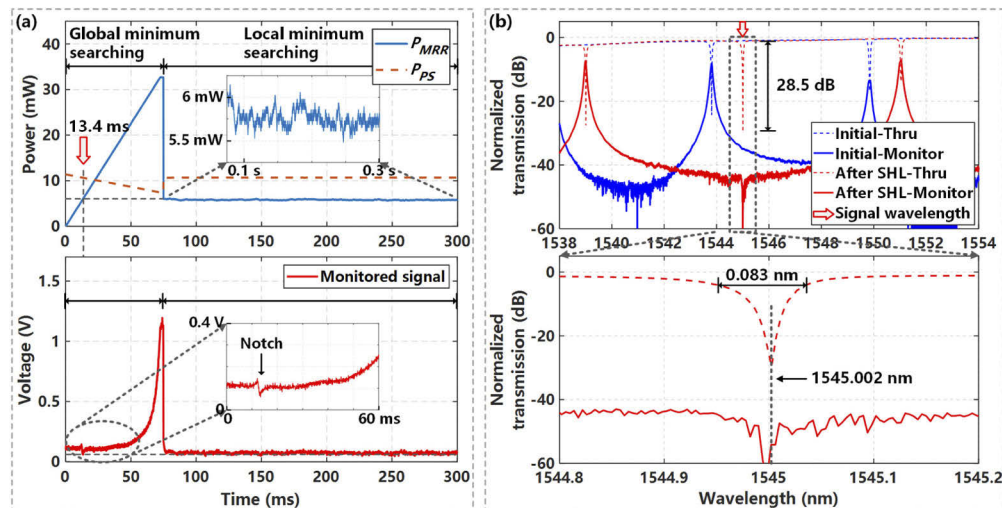


Fig. 6. (a) Heating powers and monitored signal during the locking process. Signal wavelength is 1545 nm. The inset shows the variation of P_{MRR} in the local minimum searching sub-process. (b) Measured transmission spectra at the initial state and after locking. P_{MRR} and P_{PS} are set to be 0 mW at the initial state.

signal at ~ 75 ms is maximized, indicating the corresponding wavelength misalignment is close to one FSR to reach the spectral peak as aforementioned. Afterwards, P_{MRR} is set to the power at 13.4 ms to minimize the amplitude of the monitored signal. Then, the monitored signal is kept at the minimal level by the local minimum searching sub-process, implying that the notch wavelength of the device is shifted to the signal wavelength. The inset shows the variation of P_{MRR} in the local minimum searching sub-process for tracking the minimal photocurrent. The two sub-processes last for 75 ms and ~ 10 s, respectively. After the locking process, the two heating powers remain unchanged.

Figure 6(b) shows the normalized transmission spectra at the initial state and after locking. At the initial state, the MRR is not tuned and the phase difference between the two arms are not compensated, so there is no notch in the spectrum at the monitoring port. After locking, a spectral notch with the transmission of ~ -60 dB is observed at the signal wavelength. The spectral fluctuations around the notch are relatively large due to the limited monitoring range of the power meter. The resonance wavelength after locking is 1545.002 nm, hence the locking error is 0.002 nm. The MRR has an FSR of 6.0 nm around 1550 nm. The extinction ratio and the 3-dB bandwidth at the through port are 28.5 dB and 0.083 nm, respectively. The Q factor of the MRR is therefore 1.9×10^4 .

The SHL method is also demonstrated for six other signal wavelengths within one FSR, i.e., from 1544 nm to 1550 nm. The transmission spectra of the device after locking are shown in Fig. 7(a). In each measurement, the resonance wavelength of the MRR is red-shifted to the signal wavelength by the SHL method. According to the transmissions of the device versus wavelength detuning in Fig. 7(b), the locking errors e are from -0.006 nm to $+0.015$ nm, and the average value of $|e|$ is 0.006 nm.

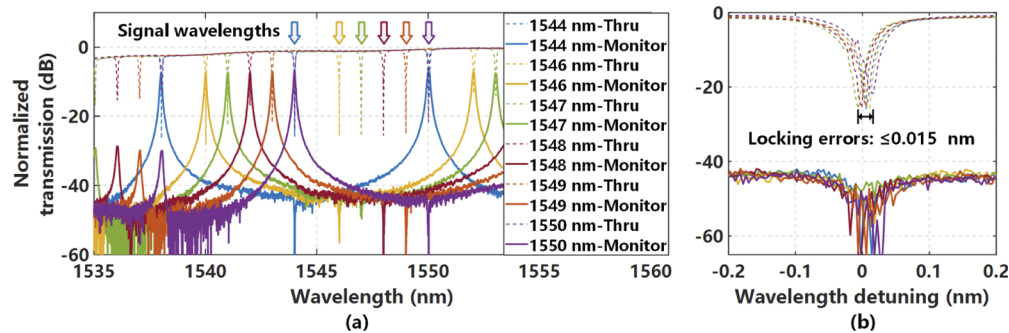


Fig. 7. Measured transmissions of the device after self-homodyne locking for six other signal wavelengths within one FSR (a) versus wavelength λ ; (b) versus wavelength detuning $\lambda - \lambda_0$. λ_0 is the signal wavelength during the locking process for each measurement.

3.3. Self-homodyne locking in the presence of input power variation

In a practical wavelength division multiplexed (WDM) system, the signal power in each wavelength channel would be affected by the power drift of the laser source, the nonuniform gain profiles of the optical amplifiers and the wavelength dependence of the optical components [30–32]. The power drift of the laser is typically small and slow, e.g., < 1 dB for 2 hours [31], while that induced by the optical amplifier is relatively large (e.g., ~ 6 dB [32]) and independent of time. Such power variations should be taken into account for MRR-based devices such as tunable MRR filters and MRR-based wavelength selective switches.

Here we performed another proof-of-concept experiment to verify the feasibility of the SHL method in the presence of input power variation. The experimental setup is shown in Fig. 8(a). The CW light beam at 1550 nm from the laser is modulated by a triangle-wave signal in a

Mach-Zehnder modulator (FTM7939EK) to cause power variation of the input light. The electrical signal is generated by a low-speed arbitrary waveform generator (AWG) (MHS-5200A), with a frequency of 100 Hz and a peak-to-peak voltage of 4.7 V. The electrical signal is biased at the quadrature point for intensity modulation. The modulated light is split into two parts by a 3-dB optical coupler. One part is fed into the device, and the other part is detected by another photodetector (PDCS986). A 1-GSa/s digital storage oscilloscope (DSO) (Tektronix TBS1002) is then used to capture the detected photocurrent signal. The rest of the experimental setup remains unchanged. Figure 8(b) is the captured signal waveform showing the input optical power variation of 8.7 dB.

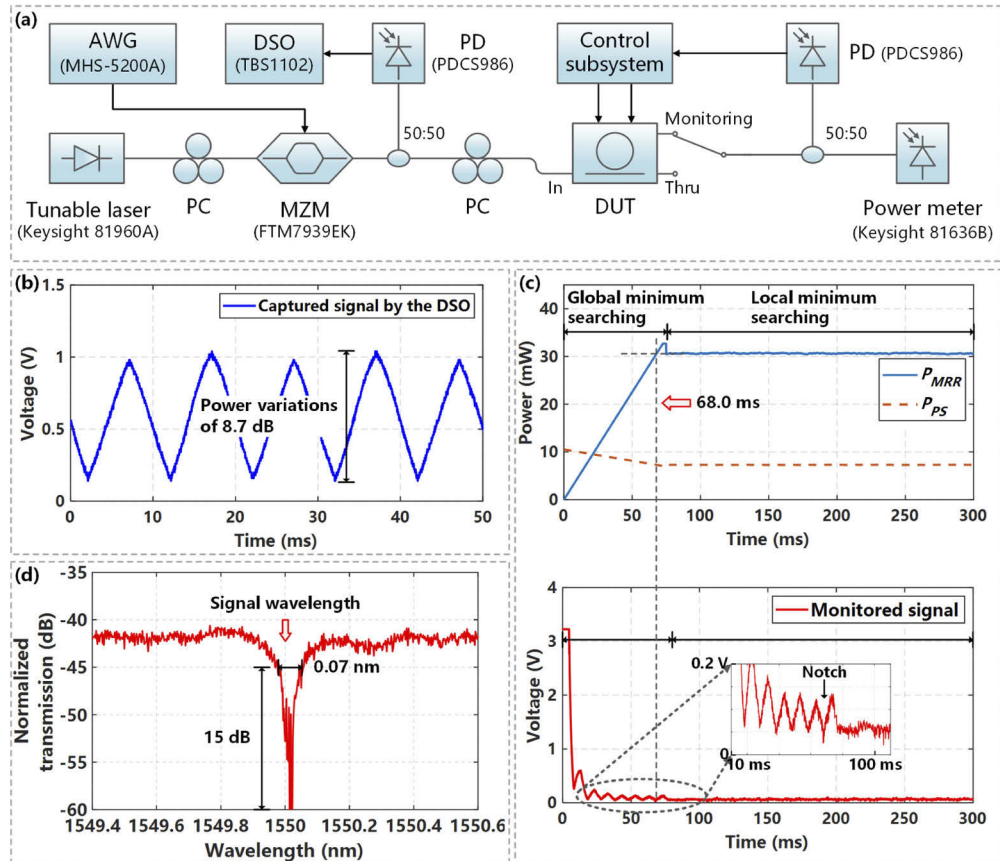


Fig. 8. (a) Experimental setup for input-optical-power insensitive wavelength locking. MZM: Mach-Zehnder modulator. AWG: arbitrary waveform generator. DSO: digital storage oscilloscope. (b) Captured signal waveform by the DSO. (c) Heating powers and monitored signal during the locking process. Signal wavelength is 1550 nm. (d) Measured transmission spectrum after locking.

The wavelength locking process is then demonstrated. The heating powers and the monitored signal during the locking process are presented in Fig. 8(c). The amplitude of the monitored signal is very large at the initial state, since the initial wavelength misalignment is $1543.808 - 1550 \approx -\text{FSR}$. In the global minimum searching sub-process, the monitored signal is minimized at 68.0 ms. During the following local minimum searching sub-process, both the heating powers and the monitored signal are almost constant, indicating that the locking process is not affected by the input optical power variation. Note that the minimal level of the monitored signal changes

with the input power. To detect the minimal level, the signal power variation shall be within the power monitoring range of the control subsystem, which is ~ 30 dB.

After the locking process, the transmission spectrum at the monitoring port is measured. The AWG is switched off before the measurement. As shown in Fig. 8(d), the notch wavelength is red-shifted to the signal wavelength of 1550 nm, with a locking error of ~ 0.012 nm. Note that the transmission variation of the spectral notch is 15 dB over a wavelength range of 0.07 nm, and the wavelength tuning speed is $\Delta P / 73 \mu\text{s} \times 0.21 \text{ nm/mW} = 0.096 \text{ nm/ms}$. The tuning time for the searching in this wavelength range is therefore $0.07 / 0.096 = 0.73 \text{ ms}$. The maximal input optical power variation in the same duration is only 1.3 dB, which is much smaller than the transmission variation around the notch and causes a negligible locking error.

Furthermore, effective wavelength locking may also be realized in the presence of both the thermal fluctuation and the laser drift, which is not demonstrated in this work due to the limit of the test equipment. Typically, the thermal fluctuation on a silicon MRR is above the millisecond regime [2,33], and the output power of a laser is stable for tens of minutes [30,31]. In the presence of both the two effects, the notch can also be located through global minimum searching, implying that the MRR is roughly locked and therefore insensitive to the power variation. Then, the local minimum searching is periodically performed to track the thermal fluctuation and minimize the locking error. Here, we assume that five feedback control periods, i.e., $< 400 \mu\text{s}$, are required for a single tracking process, whereas the thermal fluctuation is much slower. Consequently, the MRR still remains locked.

3.4. Discussion

In this section, we provide a comparison between the proposed SHL method and the conventional balanced homodyne locking (BHL) approach [22,23]. Compared to the BHL approach, the SHL method offers several benefits: 1) simplified control photonics, i.e., requiring a single photodetector; 2) automated phase calibration compensating both fabrication errors and thermal crosstalk effects; 3) potential insensitivity to in-resonator power variation since the two monitored optical beams always possess nearly the same intensities, which may be useful for MRR-based modulators. There are also several limitations for the SHL method as follows:

- (1) The SHL method may not be used for high-Q MRRs (e.g., optimized Si_3N_4 MRRs) mainly due to the limited resolution of the DACs in the control circuits. The heating powers are proportional to the square of the output voltages of the DACs and therefore range from 0 to $(2^b - 1)^2$ a.u., where b represents the digital resolution bits of the DACs. Considering a wavelength tuning range of one FSR and the use of 12-bit DACs (i.e., $b = 12$), the theoretical minimum spectral step by TO tuning is $\text{FSR} / (2^b - 1)^2 \times ((2^b - 1)^2 - (2^b - 2)^2) \approx 6 \text{ nm} / 2^{11} = 2.9 \text{ pm}$ in the worst case, i.e., the MRR is locked with the maximal heating power. We assume that accurate wavelength locking requires at least 10 spectral steps to describe the 3-dB bandwidth of the MRR and the device operates in C band, then the SHL method can lock MRRs with Q factors up to $\sim 5 \times 10^4$. The limitation of the Q factor can be broken by increasing b , i.e., using DACs with higher resolutions. For example, an MRR having a Q factor of 1.13×10^6 can be locked using a 16-bit DAC [34].
- (2) The two directional couplers along the ring would also limit the achievable Q factor of the MRR. In this work, the silicon MRR with two directional couplers exhibits a Q factor of 1.9×10^4 as aforementioned.
- (3) The monitored signal in the SHL method is not center on zero. According to Fig. 7, the monitored signal is symmetric with respect to the signal wavelength. This stands in contrast to some existing wavelength locking approaches (e.g., the BHL [22,23] and Pound-Drever-Hall [5–7] techniques) in which the monitored/error signal is asymmetric

with respect to the signal wavelength and thus the sign of the wavelength misalignment can be easily obtained. Then, for the proposed SHL method, a minimum searching algorithm implemented in a digital signal processor is used to achieve the wavelength locking in this case.

- (4) The SHL method should not be used for lasers. While the BHL method can realize the frequency stabilization of a laser source since the DC offset of the monitored signal is proportional to the Q factor of the laser, the SHL method may not work in that case. This is because the monitored signal amplitude is close to zero at the resonance wavelength, i.e., the Q factor that indicates the frequency fluctuation of the laser may not be obtained through the monitored signal.

4. Conclusion

We proposed and experimentally demonstrated a SHL method for the wavelength locking of a silicon MRR. By employing a device structure based on the self-homodyne detection and a control subsystem, the MRR can be locked to the signal wavelength based on RTPS monitoring. Two proof-of-concept experiments were performed to verify the feasibility of the proposed method in a wide wavelength range and in the presence of input power variation. The results show that this method can achieve effective wavelength locking of the MRR over a full FSR of 6 nm, and is insensitive to the input optical power variation. The locking errors in all the measurements are ≤ 0.015 nm.

Funding

Science and Technology Commission of Shanghai Municipality (17500710900); National Key R&D Program of China (2018YFE0201000) National Natural Science Foundation of China (61860206001, 61875120). Open Fund of IPOC (BUPT).

Acknowledgments

The authors would like to thank the support of device fabrication by the Center for Advanced Electronic Materials and Devices of Shanghai Jiao Tong University.

Disclosures

The authors declare no conflicts of interest.

References

1. P. Dong, Y. K. Chen, G. H. Duan, and D. T. Neilson, "Silicon photonic devices and integrated circuits," *Nanophotonics* **3**(4-5), 215–228 (2014).
2. K. Padmaraju and K. Bergman, "Resolving the thermal challenges for silicon microring resonator devices," *Nanophotonics* **3**(4-5), 269–281 (2014).
3. W. Bogaerts, P. De Heyn, T. Van Vaerenbergh, K. De Vos, S. K. Selvaraja, T. Claes, P. Dumon, P. Bienstman, D. Van Thourhout, and R. Baets, "Silicon microring resonators," *Laser Photonics Rev.* **6**(1), 47–73 (2012).
4. Y. Zhang, R. Zhang, Q. Zhu, Y. Yuan, and Y. Su, "Architecture and devices for silicon photonic switching in wavelength, polarization and mode," *J. Lightwave Technol.*, accepted (2019).
5. M. H. Idjadi and F. Aflatouni, "Integrated Pound–Drever–Hall laser stabilization system in silicon," *Nat. Commun.* **8**(1), 1209 (2017).
6. J. Chambers, "High frequency Pound–Drever–Hall optical ring resonator sensing," Master's thesis, Texas A&M University (2007).
7. E. D. Black, "An introduction to Pound–Drever–Hall laser frequency stabilization," *Am. J. Phys.* **69**(1), 79–87 (2001).
8. L. P. Barry, R. O'Dowd, J. Debau, and R. Boittin, "Tunable transform-limited pulse generation using self-injection locking of an FP laser," *IEEE Photonics Technol. Lett.* **5**(10), 1132–1134 (1993).
9. K. Hsu and S. Yamashita, "Single-polarization generation in fiber Fabry-Perot laser by self-injection locking in short feedback cavity," *J. Lightwave Technol.* **19**(4), 520–526 (2001).

10. X. Zhu, K. Padmaraju, L. W. Luo, S. Yang, M. Glick, R. Dutt, M. Lipson, and K. Bergman, "Fast wavelength locking of a microring resonator," *IEEE Photonics Technol. Lett.* **26**(23), 2365–2368 (2014).
11. X. Zheng, E. Chang, P. Amberg, I. Shubin, J. Lexau, F. Liu, H. Thacker, S. S. Djordjevic, S. Lin, Y. Luo, J. Yao, J. H. Lee, K. Raj, R. Ho, J. E. Cunningham, and A. V. Krishnamoorthy, "A high-speed, tunable silicon photonic ring modulator integrated with ultra-efficient active wavelength control," *Opt. Express* **22**(10), 12628–12633 (2014).
12. H. Jayatilika, H. Shoman, L. Chrostowski, and S. Shekhar, "Photoconductive heaters enable control of large-scale silicon photonic ring resonator circuits," *Optica* **6**(1), 84–91 (2019).
13. H. Jayatilika, H. Shoman, R. Boeck, N. A. F. Jaeger, L. Chrostowski, and S. Shekhar, "Automatic configuration and wavelength locking of coupled silicon ring resonators," *J. Lightwave Technol.* **36**(2), 210–218 (2018).
14. R. Gatdula, K. Kim, A. Melikyan, Y. K. Chen, and P. Dong, "Simultaneous four-channel thermal adaptation of polarization insensitive silicon photonics WDM receiver," *Opt. Express* **25**(22), 27119–27126 (2017).
15. Q. Zhu, X. Jiang, Y. Yu, R. Cao, H. Zhang, D. Li, Y. Li, L. Zeng, X. Guo, Y. Zhang, and C. Qiu, "Automated wavelength alignment in a 4×4 silicon thermo-optic switch based on dual-ring resonators," *IEEE Photonics J.* **10**(1), 1–11 (2018).
16. Q. Zhu, H. Zhang, R. Cao, N. Zhao, X. Jiang, D. Li, Y. Li, X. Song, X. Guo, Y. Zhang, and C. Qiu, "Wide-range automated wavelength calibration over a full FSR in a dual-ring based silicon photonic switch," in *Opt. Fiber Commun. Conf.* 2018, paper Th3C.1.
17. Q. Zhu, S. An, R. Cao, Y. Ling, and Y. Su, "Fast and wide-range wavelength locking based on a two-layer neural network in a silicon microring switch," in *Opt. Fiber Commun. Conf.* 2019, paper W1E.1.
18. Q. Zhu, X. Jiang, R. Cao, H. Zhang, C. Qiu, and Y. Su, "Multi-stage wavelength locking in a 4×4 silicon electro-optic switch based on dual-ring resonators," in *Optoelectron. Commun. Conf. & Photon. Switching Comput.* 2019, paper TuF2.5.
19. E. Timurdogan, A. Biberman, D. C. Trotter, C. Sun, M. Moresco, V. Stojanovic, and M. R. Watts, "Automated wavelength recovery for microring resonators," in *Conf. Lasers Electro-Opt.* 2012, paper CM2M.1.
20. K. Padmaraju, J. Chan, L. Chen, M. Lipson, and K. Bergman, "Thermal stabilization of a microring modulator using feedback control," *Opt. Express* **20**(27), 27999–28008 (2012).
21. Y. Li and A. W. Poon, "Active resonance wavelength stabilization for silicon microring resonators with an in-resonator defect-state-absorption-based photodetector," *Opt. Express* **23**(1), 360–372 (2015).
22. J. A. Cox, A. L. Lentine, D. C. Trotter, and A. L. Starbuck, "Control of integrated micro-resonator wavelength via balanced homodyne locking," *Opt. Express* **22**(9), 11279–11289 (2014).
23. S. Lin, X. Zheng, P. Amberg, S. S. Djordjevic, J. H. Lee, I. Shubin, J. Yao, Y. Luo, J. Bovington, D. Y. Lee, H. D. Thacker, J. E. Cunningham, K. Raj, and A. V. Krishnamoorthy, "Wavelength locked high-speed microring modulator using an integrated balanced homodyne CMOS control circuit," in *Opt. Fiber Commun. Conf.* 2016, paper Th3J.4.
24. W. A. Zortman, A. L. Lentine, D. C. Trotter, and M. R. Watts, "Bit-error-rate monitoring for active wavelength control of resonant modulators," *IEEE Micro* **33**(1), 42–52 (2013).
25. C. T. DeRose, M. R. Watts, D. C. Trotter, D. L. Luck, G. N. Nielson, and R. W. Young, "Silicon microring modulator with integrated heater and temperature sensor for thermal control," in *Conf. Lasers Electro-Opt.* 2010, paper CThJ.3.
26. A. Yariv, "Critical coupling and its control in optical waveguide-ring resonator systems," *IEEE Photonics Technol. Lett.* **14**(4), 483–485 (2002).
27. F. Liu, Q. Li, Z. Zhang, M. Qiu, and Y. Su, "Optically tunable delay line in silicon microring resonator based on thermal nonlinear effect," *IEEE J. Sel. Top. Quantum Electron.* **14**(3), 706–712 (2008).
28. Y. Su and Q. Chang, "Tunable photonic RF phase shifter using silicon microring resonator," in *Laser Resonators and Beam Control XII* 2010, paper 757912.
29. Y. Xia, C. Qiu, X. Zhang, W. Gao, J. Shu, and Q. Xu, "Suspended Si ring resonator for mid-IR application," *Opt. Lett.* **38**(7), 1122–1124 (2013).
30. Y. G. Han, J. H. Lee, S. B. Lee, L. Poti, and A. Bogoni, "Novel multiwavelength erbium-doped fiber and Raman fiber ring lasers with continuous wavelength spacing tunability at room temperature," *J. Lightwave Technol.* **25**(8), 2219–2225 (2007).
31. K. Lee, S. Do Lim, C. H. Kim, J. H. Lee, Y. G. Han, and S. B. Lee, "Noise reduction in multiwavelength SOA-based ring laser by coupled dual cavities for WDM applications," *J. Lightwave Technol.* **28**(5), 739–745 (2010).
32. M. C. Parker, A. D. Cohen, and R. J. Mears, "Dynamic holographic spectral equalization for WDM," *IEEE Photonics Technol. Lett.* **9**(4), 529–531 (1997).
33. Y. H. Chen, C. Sun, and V. Stojanovic, "Scalable electrical-optical thermal simulator for multicores with optical interconnects," in *IEEE Opt. Interconnect Conf.* 2013, paper M3A.
34. Y. Yu, H. Tang, W. Liu, X. Hu, Y. Zhang, X. Xiao, Y. Yu, and X. Zhang, "Frequency stabilization of the tunable optoelectronic oscillator based on an ultra-high-Q microring resonator," *IEEE J. Sel. Top. Quantum Electron.* **26**(2), 1–9 (2020).